Journal of Molecular Catalysis A: Chemical 323 (2010) 52–58

Contents lists available at ScienceDirect

Journal of Molecular Catalysis A: Chemical

journal homepage: www.elsevier.com/locate/molcata

Influence of the cerium precursor on the physico-chemical features and NO to NO_2 oxidation activity of ceria and ceria–zirconia catalysts

Noelia Guillén-Hurtado, Idriss Atribak, Agustín Bueno-López, Avelina García-García*

MCMA Group, Department of Inorganic Chemistry, Faculty of Sciences, University of Alicante, Campus Sant Vicent s/n, Ap. 99-E-03080 Alicante, Spain

ARTICLE INFO

Article history:
Received 18 September 2009
Received in revised form 15 February 2010
Accepted 7 March 2010
Available online 15 March 2010

Keywords:
Ceria–zirconia
Mixed oxides
Ceria
XPS
NO to NO_2 oxidation activity

ABSTRACT

The preparation of $Ce_{0.80}Zr_{0.20}O_2$ mixed oxides was conducted by coprecipitation, using either $Ce(NO_3)_3{\cdot}6H_2O$ or $(NH_4)_2Ce(NO_3)_6$ as cerium precursor. Their counterpart pure ceria samples were also prepared for comparative purposes. The samples were characterised by N_2 adsorption at −196 °C, XRD, Raman spectroscopy, XRF, H_2-TPR and XPS, establishing proper comparisons with a commercial catalyst $Ce_{0.80}Zr_{0.20}O_2$, supplied by Rhodia. The use of $Ce(NO_3)_3{\cdot}6H_2O$ leads to a Ce–Zr mixed oxides with ceria-like structure, Ce-enrichment on the surface and a bi-modal H_2-TPR profile, not expected for a true solid solution. On the contrary, a t″ structure was identified when using $(NH_4)_2Ce(NO_3)_6$ as precursor, exhibiting improved oxygen mobility and Zr-enrichment on the particle surface. These findings are in accordance with the solution chemistry of the Ce-species involved. When two pure ceria samples are compared, the most important difference is the very low surface area of CeO_2 prepared from the Ce^{4+} precursor (5 m^2/g) compared with CeO_2 prepared from the Ce^{3+} precursor (57 m^2/g). The Ce–Zr mixed oxides prepared from the precursor $(NH_4)_2Ce(NO_3)_6$ shows the highest NO oxidation capacity among the samples prepared in this study. The NO oxidation capacity to NO_2 seems to be dependent not only on the BET surface area of the catalyst but also on the Ce/Zr atomic surface ratio and probably, the redox properties of the catalysts, when mixed oxides with the same nominal composition are compared.

1. Introduction

CeO_2–ZrO_2 is not only one of the most important catalytic supports due to its use in the three-way catalysts but also an interesting catalyst by itself. Ceria–zirconia mixed oxides exhibit significant thermal stability, good redox characteristics and catalytic activity towards several oxidation reactions [1]. Having these properties, these materials have been tested for oxidation of hydrocarbons [2] and CO [3], CO_2 methane reforming [4] and partial oxidation of methane [5]. Recently, the study of the catalysed oxidation of NO to NO_2 has acquired significance due to its role in several catalytic processes, such as soot combustion under NO_x/O_2 [6–8], NO_x storage/reduction strategy [9], selective catalytic reduction of NO_x with hydrocarbons [10] and so on.

In this line, it becomes interesting to optimise the variables of preparation of CeO_2–ZrO_2 materials, possibly avoiding the use of Pt and Pd whose prices are both high and highly fluctuating [11], not only in order to obtain new lower-cost catalytic materials but also to design environmental-friendly routes of synthesis with a minimal or null disposal of organic solvents and/or surfactants.

It is known that the preparation method can remarkably affect the textural and chemical behaviour at a single sample ceria/zirconia composition [12]. Several synthetic methods have been employed for the preparation of these compounds: hydrothermal synthesis, sol–gel methods, surfactant-assisted routes and reversed microemulsion, among others [1]. However, one of the most straightforward methods both in minimal use of reactants and procedure is the coprecipitation [13].

In a previous publication [14], a mixed oxide of composition $Ce_{0.76}Zr_{0.24}O_2$ obtained by the coprecipitacion method by using a Ce^{3+} precursor showed nearly the same activity towards NO oxidation to NO_2 (TPR conditions) as bare ceria, both samples being calcined at 500 °C. Nevertheless, the mixed oxide was preferable to pure ceria since it presented enhanced thermal stability. A detailed physico-chemical characterisation of this mixed oxide revealed a certain degree of inhomogeneous distribution of cerium and zirconium cations. This was inferred by XPS analysis, providing Ce-enrichment on the particle surface. This heterogeneity was concordant with a bi-modal H_2-TPR profile, not expected for a true solid solution. These peculiarities should be motivated by the choice of a Ce^{3+} precursor instead of a Ce^{4+} precursor to carry out the coprecipitation of the cerium hydroxide along with the zirconium hydroxide, as reported by Letichevsky et al. [13]. In that study the use of $Ce(NO_3)_3$ as precursor led to the formation of separated ceria and zirconia phases whereas a solid

* Corresponding author. Tel.: +34 96590 9419; fax: +34 96590 3454.
E-mail address: a.garcia@ua.es (A. García-García).

1381-1169/$ – see front matter © 2010 Elsevier B.V. All rights reserved.
doi:10.1016/j.molcata.2010.03.010

solution was obtained by using $(NH_4)_2Ce(NO_3)_6$ in conducting coprecipitation [13].

With a view to shedding light on these issues and to analysing the influence of the cerium precursor on the physico-chemical properties of the mixed oxides obtained and on their catalytic activity for NO oxidation, ceria–zirconia mixed oxides with the same nominal composition ($Ce_{0.80}Zr_{0.20}O_2$) were prepared by the coprecipitation method, using a Ce^{3+} or a Ce^{4+} precursor, along with their control pure ceria samples, to establish proper comparisons. The results of the physico-chemical characterisation as well as the catalytic activity towards NO oxidation to NO_2 are presented and discussed in the current paper.

2. Experimental

2.1. Catalyst preparation

Two $Ce_{0.80}Zr_{0.20}O_2$ mixed oxides were synthesised by the coprecipitation route from either $Ce(NO_3)_3{\cdot}6H_2O$ (supplied by Aldrich, 99% of purity) or $(NH_4)_2Ce(NO_3)_6$ (supplied by Panreac, 99% of purity). The required amounts of $ZrO(NO_3)_2{\cdot}xH_2O$ (supplied by Aldrich, Tech. grade) and the cerium precursor were dissolved in water and the hydroxides were precipitated by dropping an ammonia solution to keep the pH about 9 and subsequent filtering. The precipitates were dried at 110 °C in air overnight and calcined in air for 1 h at 500 °C. Pure CeO_2 samples prepared with the Ce^{3+} or Ce^{4+} precursor were also obtained following the same procedure. The samples prepared with the Ce^{3+} precursor are denoted by "$Ce_{0.80}Zr_{0.20}O_2$ (Ce^{3+})" and "CeO_2 (Ce^{3+})" and those prepared with the Ce^{4+} precursor are denoted by "$Ce_{0.80}Zr_{0.20}O_2$ (Ce^{4+})" and "CeO_2 (Ce^{4+})". A $Ce_{0.80}Zr_{0.20}O_2$ commercial sample supplied by Rhodia France (La Rochelle) and obtained by nitrate precursors was also used for comparative purposes. This sample is denoted by "Rhodia".

2.2. Characterisation techniques

The BET surface areas of the samples were determined by multi-point N_2 adsorption at −196 °C using an automatic Autosorb-6B (Quantachrome equipment). The samples were previously degassed for 4 h at 250 °C under vacuum.

Powder XRD patterns were recorded in a Bruker D8 advance diffractometer, using CuK_α radiation. Spectra were registered between 10 and 80° (2θ) with a step of 0.02° and a time per step of 3 s. The estimation of crystal size has been carried out with the following Williamson-Hall's equation:

$$\beta_{Total} = \beta_{Size} + \beta_{Strain} = \frac{0.9\lambda}{D\cos\theta} + \frac{4(\Delta d)\sin\theta}{d\cos\theta}$$

where β_{Total} is the full width half maximum of the XRD peaks and Δd is the difference of the d spacing corresponding to a typical peak. A plot of $\beta_{Total}{\cdot}\cos\theta$ against $4\sin\theta$ yields the average crystal size from the intercept value.

The introduction of foreign cations within the lattice of ceria deforms the structure and affects the shape of the XRD peaks. The Williamson-Hall's equation separates the effects of size and strain in the crystals, and is more convenient than the Scherrer's equation for the estimation of crystal size of mixed oxides [14].

Raman spectra were obtained in a Bruker RFS 100/S Fourier Transform Raman Spectrometer with a variable power Nd:YAG laser source (1064 nm). Sixty-four scans at 85 mW laser power (70 mW on the sample) were recorded and no heating of the sample was observed under these conditions.

Semi-quantitative chemical analysis of the sample was performed by XRF in a Philips Magix Pro spectrometer provided with analytic software SuperQ.

XPS characterisation of the catalysts was carried out in a VG-Microtech Multilab electron spectrometer using a MgK_α (1253.6 eV) radiation source. To obtain the XPS spectra, the pressure of the analysis chamber was maintained at 5×10^{-10} mbar. The binding energy (BE) and the kinetic energy (KE) scales were adjusted by setting the C 1s transition at 284.6 eV, and BE and KE values were determined with the Peak-fit software of the spectrometer. The electronic transitions $Zr_{3d5/2}$, $Ce_{3d5/2}$, $Ce_{3d3/2}$, and the satellite cerium peak centred at 917 eV were used to determine the surface concentration of zirconium and cerium. The proportion of Ce^{3+} cations with regard to the total cerium was calculated as the ratio of the sum of the intensities of the u_0, u', v_0 and v' bands to the sum of the intensities of all the bands [15]:

$$Ce^{3+}\ (\%) = \frac{v_0 + v' + u_0 + u'}{\Sigma(v+u)} \quad (2)$$

The reducibility of the fresh catalysts was examined by H_2-temperature-programmed reduction (H_2-TPR) in a Micromeritics Pulse ChemiSorb 2705 device consisting of a tubular quartz reactor coupled to a TCD detector in order to monitor H_2 consumption. The reducing gas used was 5% H_2 in Ar, with a flow rate of 35 ml/min. The temperature range explored was from room temperature to 900 °C at a heating rate of 10 °C/min. A CuO reference sample (supplied by Micromeritics) was used to quantify H_2 consumption.

2.3. Catalytic oxidation of NO to NO_2

The catalytic tests were performed in a tubular quartz reactor coupled to specific NDIR-UV gas analysers for NO, NO_2 and O_2 monitoring. The selected catalyst of 80 mg was diluted with SiC to avoid pressure drop. The gas mixture used comprised 500 ppm NO_x, 5% O_2 and balance N_2, and the gas flow was fixed at 500 ml/min (GHSV = 30,000 h^{-1}). The experimental set-up has been designed in order to ensure that the proportion of NO_2 in the NO + O_2 mixture fed to the reactor is null.

These tests consisted of temperature programmed reactions, where the temperature was increased from room temperature to 700 °C at 10 °C/min under the reactive atmosphere, with the purpose of quantifying the NO to NO_2 oxidation capacity of the samples. A blank experiment was carried out under the aforementioned experimental conditions but with the empty reactor.

3. Results and discussion

3.1. XRD, N_2 adsorption and XRF characterisation

XRD patterns of the four solids synthesised along with that of the Rhodia sample are presented in Fig. 1. All samples exhibit only peaks which could refer to the fluorite structure of CeO_2, and separate zirconia phases are not observed for the three samples with $Ce_{0.80}Zr_{0.20}O_2$ composition. The position of the XRD peaks is equal for the samples CeO_2 (Ce^{3+}), CeO_2 (Ce^{4+}) and $Ce_{0.80}Zr_{0.20}O_2$ (Ce^{3+}), while they are shifted to higher angles for the samples $Ce_{0.80}Zr_{0.20}O_2$ (Ce^{4+}) and Rhodia. Such a shift is usually related to a change in the lattice parameter due to the introduction of small Zr^{4+} cations within the CeO_2 lattice, and has been currently taken as an indication of a CeO_2–ZrO_2 solid solution formation [13,16].

The same phase assignments by XRD were reported by Letichevsky et al. [13] for $Ce_{0.75}Zr_{0.25}O_2$ mixed oxides prepared also from tri- and tetravalent cerium precursors. Conversely, Rossignol et al. [17] and Hori et al. [16] found phase segregation (cubic ceria and tetragonal zirconia) by XRD for a mixed oxide of identical composition prepared from the Ce^{3+} precursor.

Table 1 compiles the estimation of the crystal sizes and the BET surface areas for the five samples used in this study. Using the Scherrer's equation to estimate the size by peak broadening sup-

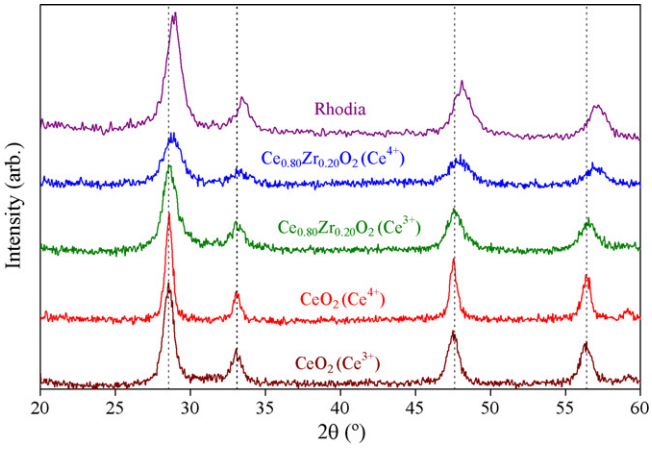

Fig. 1. XRD characterisation of the catalysts.

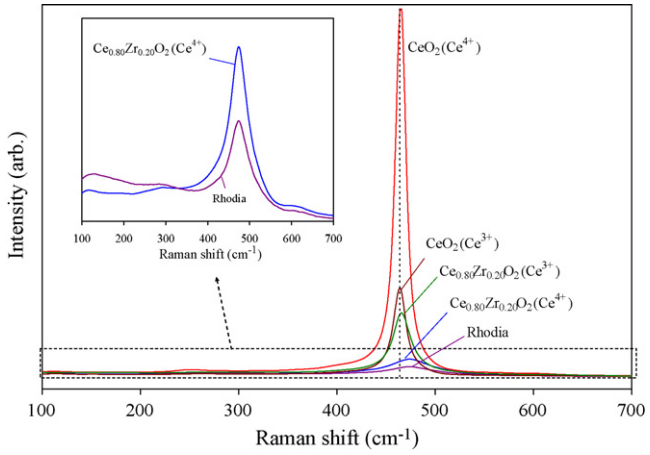

Fig. 2. Raman characterisation of the catalysts (inset of Fig. 2: zoom for Rhodia and $Ce_{0.80}Zr_{0.20}O_2$ (Ce^{4+}) sample spectra).

poses the assumption that the crystal size effects are the only source of peak broadening, but it is known that doping a ceria lattice with zirconia induces uniform strain in the lattice as the material is elastically deformed [16]. As the Williamson-Hall's equation separates the effect of size and strain in the crystal, it is more convenient for estimations relative to mixed oxides. By comparing the crystal sizes of the pure oxides (13 and 20 nm for CeO_2 (Ce^{3+}) and CeO_2 (Ce^{4+}), respectively) with those of the mixed oxides (7 and 6 nm for $Ce_{0.80}Zr_{0.20}O_2$ (Ce^{3+}) and $Ce_{0.80}Zr_{0.20}O_2$ (Ce^{4+}), respectively) it is proved that crystal growth is hindered by incorporating zirconium within the ceria framework. Similar trends were found by Letichevsky et al. [13]; CeO_2 yielded a particle diameter of 5.7 nm and the corresponding solid solution yielded 3.9 nm (estimated by means of the Rietveld's method). The larger crystal sizes found for the mixed oxides obtained in this study compared to those obtained by Letichevsky et al. [13] must be due to the differences in the steps of the preparation protocols used. On the other hand, the data in Table 1 reveals that the cerium precursor does not affect significantly the crystal size of the mixed oxides while it has a strong effect on pure ceria samples, smaller size being obtained with the Ce^{3+} precursor for bare ceria samples.

Accordingly, the BET area decreases by an order of magnitude for CeO_2 (Ce^{3+}) with regard to CeO_2 (Ce^{4+}) (57 and 5 m^2/g, respectively) while they are not very different for both mixed oxides prepared in this study (68 and 57 m^2/g for $Ce_{0.80}Zr_{0.20}O_2$ (Ce^{3+}) and $Ce_{0.80}Zr_{0.20}O_2$ (Ce^{4+}), respectively). This observation is in agreement with the data reported by Rossignol et al. [17] for $Ce_xZr_{1-x}O_2$ mixed oxides calcined at 780 °C, where the BET surface area slowly diminished as the atomic fraction of cerium (x) increased from 0.75 and 1.

Semi-quantitative chemical analysis performed on the samples by XRF revealed a fairly similar nominal composition for both mixed oxides in Ce and Zr. Also Cu, Fe and Ca were identified as very minor components, assessing no differences in impurities by using different cerium precursors.

Table 1
Crystal sizes, BET surface areas and H_2 consumed amounts from surface reduction by H_2 of the samples.

Sample	Crystal size (nm)	BET surface area (m^2/g)	Surface reduction ($\mu mol\ H_2/g_{sample}$)
CeO_2 (Ce^{3+})	13	57	145
$Ce_{0.80}Zr_{0.20}O_2$ (Ce^{3+})	7	68	157
CeO_2 (Ce^{4+})	20	5	60
$Ce_{0.80}Zr_{0.20}O_2$ (Ce^{4+})	6	57	454
Rhodia	14	113	–

3.2. Raman spectroscopy characterisation

According to the classification of phases in the CeO_2–ZrO_2 binary system, a cubic structure is expected for a composition range (% mol in Ce) of 80–100% and a t″ metastable tetragonal phase is expected in the range of 65–80%. It is intermediate between t′ and c. The t″ phase shows no tetragonality of the cation sublattice and exhibits an oxygen displacement from ideal fluorite sites [1]. Therefore, the mixed oxides obtained in this study (80%) are in the threshold value. Such differences in the crystalline structure can be distinguished by Raman spectroscopy.

Raman spectra of the five samples analysed are displayed in Fig. 2. For all of them, a sharp band is observed at about 465 cm^{-1} assigned to the fluorite structure, which is a cubic structure with space group *Fm*3*m*. The intensity of the signal is the highest one for the sample CeO_2 (Ce^{4+}), in agreement with the largest crystal size of this sample (see data in Table 1). By comparing the three mixed oxides, both the broadening of this F_{2g} peak and its marked decrease in intensity exhibited by Rhodia sample and $Ce_{0.80}Zr_{0.20}O_2$ (Ce^{4+}) compared to $Ce_{0.80}Zr_{0.20}O_2$ (Ce^{3+}) have to be connected with an increase in disorder in the fluorite structure and cell contraction and/or existence of oxygen vacancies [1].

Both the position of the main band at around 465 cm^{-1} and that of the smaller bands that could appear at lower Raman shifts (see the inset zoom of Fig. 2) provide information about the actual structure of the mixed oxides. The position of the main band is almost equal for the samples CeO_2 (Ce^{4+}), CeO_2 (Ce^{3+}) and $Ce_{0.80}Zr_{0.20}O_2$ (Ce^{3+}) (464–466 cm^{-1}) whereas it is moved to higher Raman shifts for the samples $Ce_{0.80}Zr_{0.20}O_2$ (Ce^{4+}) and Rhodia (473.5 cm^{-1}).

The Raman spectra of the samples $Ce_{0.80}Zr_{0.20}O_2$ (Ce^{4+}) and Rhodia are consistent with a t″ structure. This is deduced from the up-shifted main band, which is in accordance with other values reported for solid solutions in the literature [12,13], and from the presence of very low and broad bands at around 120 and 300 cm^{-1}, owing to the tetragonal displacement of the oxygen from the ideal fluorite structure which occurs due to the zirconium insertion into the CeO_2 lattice. The shoulder at 620 cm^{-1} could be ascribed to a localised substitutional defect vibration, according to Martínez-Arias et al. [18].

On the contrary, according to the structural characterisation presented so far, a cubic structure is assigned to the mixed oxide prepared from a Ce^{3+} precursor, since this sample neither exhibits displacement of the main band towards a higher Raman shift with regard to pure ceria samples nor weak bands at around 120 and

Table 2
Data from surface analysis by XPS.

Sample	$Ce^{3+}/(Ce^{3+}+Ce^{4+})$ (%)	Ce/Zr surface atomic ratio	O/(Ce + Zr) or O/Ce surface atomic ratio
CeO_2 (Ce^{3+})	28.2	–	3.6
$Ce_{0.80}Zr_{0.20}O_2$ (Ce^{3+})	32.3	5.9 (4.0)	3.0
CeO_2 (Ce^{4+})	34.8	–	3.0
$Ce_{0.80}Zr_{0.20}O_2$ (Ce^{4+})	34.6	2.4 (4.0)	2.8
Rhodia	34.0	3.1 (4.0)	2.8

300 cm^{-1}, attributable to tetragonal displacement of the oxygen from the ideal fluorite structure [19].

3.3. H_2-TPR characterisation

The results obtained by means of H_2-TPR are reported in Fig. 3, where different behaviour between both pure oxides and both mixed oxides are noticed. The TPR profiles of the ceria samples showed two peaks usually reported for this pure oxide. The low-temperature peak located between 550 and 650 °C is attributed to surface reduction of the solid, and the high temperature peak between 720 and 920 °C is due to bulk reduction. This double-peak profile is explained according to the idea that oxygen mobility is relatively slow in bulk of pure ceria [20].

In addition to the surface and bulk reduction peaks, some of the profiles included in Fig. 3 show a third peak below 500 °C which could be ascribed to the desorption of adsorbed species, such as carbonate-like species, CO_2 and water. It is important to outline that, in addition to the aforementioned species, a considerable number of surface OH groups can exist on ceria-based samples [1] and some authors attribute this peak to the dehydroxylation of ceria [21].

In agreement with the literature, the area of the surface reduction peak is more pronounced for the pure ceria sample CeO_2 (Ce^{3+}), with BET surface area of 57 m^2/g, than for the sample CeO_2 (Ce^{4+}), with much lower BET area (5 m^2/g). In addition, the bulk reduction peak is slightly displaced at lower temperatures, as well as exhibiting a superior area, for CeO_2 (Ce^{3+}) than for CeO_2 (Ce^{4+}). These differences between the BET areas and redox properties of both ceria samples could be attributed to the different behaviour of each precursor during the calcination step. During $Ce(NO_3)_3{\cdot}6H_2O$ (Ce^{3+} precursor) calcination, the nitrate decomposition, with NO_x and O_2 released (and of course the O_2 atmosphere due to the air calcination) lead to the oxidation of Ce^{3+} to Ce^{4+} to yield CeO_2. On the contrary, this oxidation step does not occur during $(NH_4)_2Ce(NO_3)_6$ (Ce^{4+} precursor) calcination. The oxidation of Ce^{3+} to Ce^{4+} seems to be beneficial for the ceria features, giving a higher surface area and increased reducibility with regard to ceria obtained by Ce^{4+} precursor calcination, which seems to suffer a higher sintering.

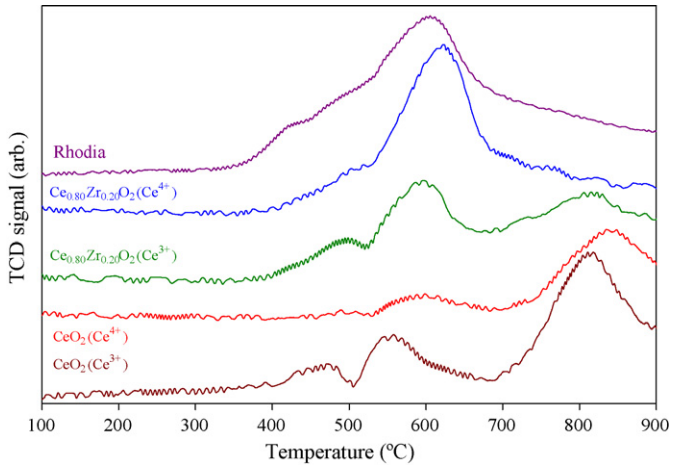

Fig. 3. H_2-TPR profiles of the catalysts.

Important differences are also noted in the H_2-TPR profiles (Fig. 3) of mixed oxides prepared from different cerium precursors. For ceria–zirconia mixed oxides, it is suggested that the high oxygen mobility in the bulk leads to a single reduction feature [22]. In agreement with this idea, a unique reduction peak is observed for the samples $Ce_{0.80}Zr_{0.20}O_2$ (Ce^{4+}) and Rhodia (Fig. 3b). This is consistent with the Raman spectroscopy findings. The t″ phase was identified for both mixed oxides and proper solid solutions formation was inferred, with good oxygen mobility. In contrast, a bi-modal profile, not expected for a solid solution, is exhibited by the sample $Ce_{0.80}Zr_{0.20}O_2$ (Ce^{3+}), rather similar to that of pure CeO_2 (Ce^{3+}). This behaviour is consistent with XRD and Raman spectroscopy data, since evidence for solid solution formation was not obtained for the sample $Ce_{0.80}Zr_{0.20}O_2$ (Ce^{3+}).

The amount of H_2 consumed in the reduction of the samples surface was calculated, and the data obtained are compiled in Table 1. The amount of H_2 consumed by the sample $Ce_{0.80}Zr_{0.20}O_2$ (Ce^{4+}) is much higher than that amount estimated for $Ce_{0.80}Zr_{0.20}O_2$ (Ce^{3+}), even though the latter presents a slightly higher surface area, and also is much higher than values obtained with both pure ceria samples. These results corroborate the good oxygen mobility attained with the ceria–zirconia mixed oxides prepared with the Ce^{4+} precursor, thus allowing a fast oxide anion migration from the bulk to the surface. The amount of H_2 consumed in the surface reduction of the sample $Ce_{0.80}Zr_{0.20}O_2$ (Ce^{4+}) is in the same order of magnitude as the amount consumed by a sample prepared by Letichevsky et al. [13] also from a Ce^{4+} precursor and with the same composition. The higher value obtained by these authors (692 μmol/g-sample) in comparison with the sample prepared in the current study could be accounted for by the higher surface area achieved by Letichevsky et al. (126 m^2/g versus 57 m^2/g).

3.4. XPS characterisation

To study in depth the surface features of the samples and attempt to correlate them with the influence of the cerium precursor, characterisation was pursued by XPS. The estimation of the Ce^{3+} percentages and the Ce/Zr, O/Ce and O/(Ce + Zr) atomic surface ratios is compiled in Table 2.

The Ce^{3+} surface percentages measured are quite similar for all the samples, ranging in a narrow interval of values between 28.2 and 34.8%. The presence of Ce^{3+} cations in samples prepared from the Ce^{4+} precursor is attributed to the reduction of the Ce^{4+} cations under the conditions of the XPS analysis. It is known that CeO_2 can suffer spontaneous reduction at room temperature during XPS measurements by action of the X-ray irradiation combined with the ultra high vacuum environment. This reduction has been reported to be strongly influenced by the composition and type of material [1]. The samples prepared from the Ce^{3+} precursor also exhibited a mixture of Ce^{3+} and Ce^{4+} cations at the surface, which confirms that part or all the Ce^{3+} cations of the nitrate precursor were oxidised to Ce^{4+} cations during calcination in air at 500 °C. In this case, the reducing conditions in the XPS experiments are also expected to contribute to Ce^{3+} formation, and therefore, the actual percentages of (+3) cations could be lower than the values obtained.

Valuable information provides the analysis of the Ce/Zr ratio for the mixed oxides studied. Taking into account that the nominal ratio is 4, if the mixed oxides presented a homogeneous atomic distribution, this would also be the surface ratio value. Even though the samples $Ce_{0.80}Zr_{0.20}O_2$ (Ce^{3+}) and $Ce_{0.80}Zr_{0.20}O_2$ (Ce^{4+}) were prepared by an identical method, with only the cerium precursor varied, this parameter is very different from each other. The mixed oxide prepared from the Ce^{3+} precursor presents a Ce/Zr value of 5.9, reflecting Ce-enrichment at the particles surface and a Zr-rich core. This degree of cerium enrichment on surface seems to be reproducible, since a sample $Ce_{0.76}Zr_{0.24}O_2$ (Ce^{3+}) was prepared in a previous work, following the same procedure used in the current study with the only difference in the calcination time (3 h instead of 1 h), showed a Ce/Zr surface ratio of 5.0 [14]. The normalisation of both values in terms of their nominal compositions provided a Ce-enrichment factor of 1.6 for that sample of a previous study and 1.5 for the sample prepared in the current study thus proving the reliability of the results and excluding effects derived from erroneous experimentalism. On the other hand, the sample $Ce_{0.80}Zr_{0.20}O_2$ (Ce^{4+}) as well as the Rhodia sample provided evidence for Zr-enrichment on the surface, with Ce/Zr surface ratios of 2.4 and 3.1, respectively. Zr-enrichment on the surface of a sample with composition $Ce_{0.75}Zr_{0.25}O_2$ prepared from a Ce^{4+} precursor by the coprecipitation method was supported by EDS data as also reported by Hori et al. [16].

Additional information regarding the surface oxidation state was also extracted from the XPS analysis. The ratio between the surface oxygen concentration and the zirconium and/or cerium concentrations was calculated and the results obtained are compiled in Table 2. The values ranged from 2.8 to 3.6. Since a value of 2 would be expected for a fully oxidised surface with an oxidation state of Ce^{4+} for all the cerium cations, the analysis clearly indicates an excess of surface oxygen. A similar conclusion was reported by Nelson and Schulz [23], obtaining a value of 2.7 for a $Ce_{0.80}Zr_{0.20}O_2$ mixed oxide prepared also by coprecipitation from $(NH_4)_2Ce(NO_3)_4$ and subsequent annealing. This value is in agreement with that obtained for the samples $Ce_{0.80}Zr_{0.20}O_2$ (Ce^{4+}) and Rhodia (2.8). This excess of oxygen at the surface could be attributed to the presence of a surface layer of adsorbed species, such as carbonate-like species, CO_2 and water. This is further supported by the detection of surface carbon by XPS both in the current study and in that of Nelson et al. [23], and would explain the peak observed in H_2-TPR profiles (Fig. 3) below 500 °C.

By comparing the O/Ce value of both ceria samples prepared in the current study and the ratios (O/Ce + Zr) for the mixed oxides, it can be concluded that the solids prepared from the Ce^{3+} precursor present a superior excess of oxygen than those prepared from the Ce^{4+} precursor.

The different distribution of elements on the surface of the samples prepared in the current study, as deduced by XPS, can be explained by careful analysis of the solution chemistry of the zirconium and cerium species involved in the different steps of the preparation procedure of samples. For the mixed oxide $Ce_{0.80}Zr_{0.20}O_2$ (Ce^{3+}), it is important to take into account that the solubility constant (K_{sp}) of $Zr(OH)_4$ is several orders of magnitude lower than that of $Ce(OH)_3$ (2×10^{-48} and 1.5×10^{-20}, respectively) [24], thus inducing a faster precipitation of zirconium hydroxide during the coprecipitation step of Ce^{3+} and Zr^{4+} in alkali media. Thus, the nuclei of the particles will be rich in zirconium and the outer part will have a prominent Ce-enrichment due to Zr depletion in the aqueous phase at the final stages of the precipitation process. This leads to a core/shell structure, different from a solid solution structure, with a heterogeneous distribution of cations, well-proved by XPS surface data. The main phase of such structure is cubic ceria, as deduced from structural analysis. This proposed structure is also congruent with the bi-modal H_2-TPR profile of the mixed oxide $Ce_{0.80}Zr_{0.20}O_2$ (Ce^{3+}). It is worth stressing that its surface peak area/bulk peak area ratio is very different from that of the control pure ceria CeO_2 (Ce^{3+}) (1.40 versus 0.41). The low area of the bulk peak for the mixed oxide $Ce_{0.80}Zr_{0.20}O_2$ (Ce^{3+}) can also be understood by the important Zr-enrichment in the bulk of the particle.

Other authors, such as Wu et al. [25] also suggested a shell/core structure for a ceria–zirconia samples prepared by means of adding firstly zirconia into aqueous ammonia and subsequent addition of $(NH_4)_2Ce(NO_3)_6$, yielding a calcined solid with very structural features than that obtained in the present study: the Ce/Zr surface atomic ratio higher than that of the nominal ratio and a bi-modal H_2-TPR profile ascribed to a diffusional resistance, causing firstly the reduction of Ce^{4+} surface and separately the reduction with oxygen supplied from the bulk.

On the other hand, it is described in the literature [26] that the local structure around both Ce and Zr for CeO_2–ZrO_2 samples can be investigated by XAFS method in order to clarify the cation–cation network (cation = Ce, Zr) and the oxygen environment around the cation. Conventional characterisations cannot achieve exact information about the homogeneity at the atomic level for Ce and Zr atoms in the ceria–zirconia samples.

Opposite situation can be inferred from the characterisation study performed with $Ce_{0.80}Zr_{0.20}O_2$ (Ce^{4+}). K_{sp} for $Ce(OH)_4$ is 4×10^{-51} [24], which is much closer to that of $Zr(OH)_4$ (2×10^{-48}). This leads to a more homogeneous coprecipitation with solid solution formation and good oxygen mobility due to an effective insertion of the foreign cation in the ceria lattice, despite the cerium depletion in the very late stages of the precipitation, since $Ce(OH)_4$ is slightly more insoluble than $Zr(OH)_4$.

Other aspects, such as the complex and distinct solution chemistry of ceric ions resultant from using a Ce^{3+} or a Ce^{4+} precursor, point also the same direction. The coordination chemistry of the large electropositive Ce^{3+} ions is complicated in solution. However, it is likely that the aqueous solution contains the $[Ce(H_2O)_9]^{3+}$ cation [27] which would not benefit the proximity of the cationic zirconyl (ZrO^{2+}) because of electrostatic repulsion. In contrast, an electrostatic attraction is expected when the $(NH_4)_2Ce(NO_3)_6$ precursor is used, as its hydrolysis yields a 12-coordinated Ce anion $[Ce(NO_3)_6]^{2-}$, characterised by 12 oxygen atoms from 6 bidentade nitrate ions surrounding Ce^{4+} [27]. Such effects would facilitate the proximity between both species before the addition of ammonia.

3.5. Catalytic oxidation of NO to NO_2

The influence of the cerium precursor on the NO oxidation capacity of the pure and mixed oxides prepared in this study has been studied under a gas mixture with NO and O_2. Fig. 4 presents the results obtained in these experiments. Fig. 4(a and b) depicts the NO_x elimination profiles and the NO_2 percentage in the outlet gas mixture respectively, as a function of temperature.

As observed in Fig. 4a, all the samples studied remove NO_x from the gas stream, and this removal is attributed to NO_x chemisorption on the cerium-based oxides. The nitrogenated-species formed on the cerium samples upon NO_x chemisorption (ad-NO_x species) are stable under the experimental conditions. The samples CeO_2 (Ce^{3+}), $Ce_{0.80}Zr_{0.20}O_2$ (Ce^{3+}) and $Ce_{0.80}Zr_{0.20}O_2$ (Ce^{4+}) show the same NO_x removal profile, and the most outstanding point deduced from Fig. 4a is the lowest NO_x chemisorption capacity, joined to a shift towards higher temperatures of the NO_x removal curve shown by the sample CeO_2(Ce^{4+}), compared with the other three samples. The lowest NO_x chemisorption capacity of the sample CeO_2(Ce^{4+}) is in accordance with its lower surface area (5 m^2/g versus 57–68 m^2/g).

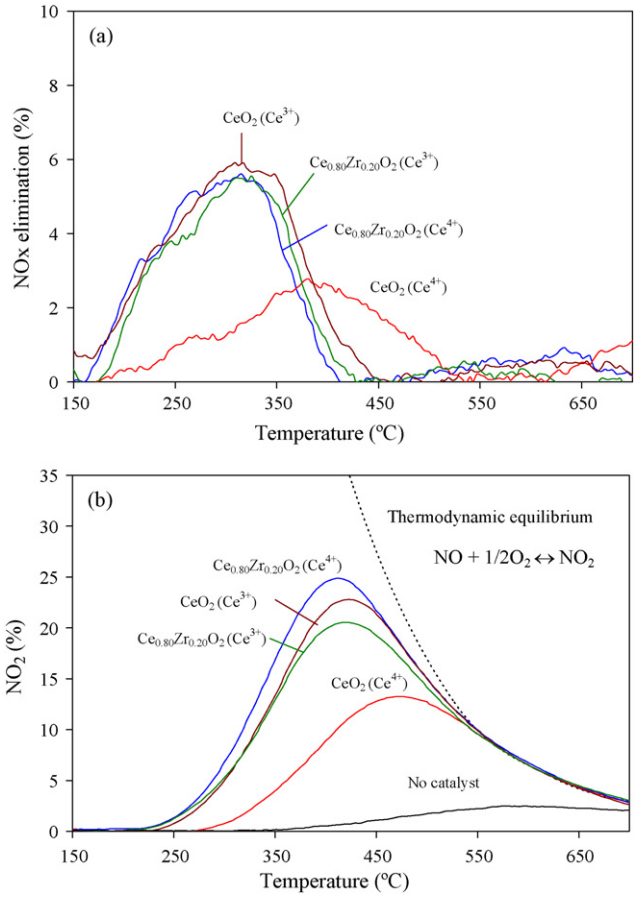

Fig. 4. Catalytic tests: (a) NO_x elimination profiles and (b) NO_2 production profiles.

In addition to NO_x chemisorption on the pure and doped cerium samples, the interaction of the $(NO + O_2)$ gas mixture with the different catalysts leads to the oxidation of NO to NO_2, as observed in Fig. 4b. It is important to remember that the experimental set-up used in these experiments was designed to ensure that the proportion of NO_2 in the $NO + O_2$ mixture fed to the reactor is null, as deduced from the baseline value of the NO_2 level below 250 °C in all the experiments. The NO oxidation reaction is thermodynamically favoured at low-temperature but kinetically restricted, and hence, both the action of a catalyst and the increase in temperature accelerate the oxidation of NO. In the absence of catalyst, the NO_2 level is low, and the highest level reached is about 2% at 600 °C. All the cerium catalysts prepared in this study are able to accelerate the oxidation of NO to NO_2. Above a certain temperature (250–300 °C) the NO_2 level increases and, once the thermodynamic equilibrium of the NO oxidation reaction is reached, the NO_2 level decreases following thermodynamics.

From a quantitative point of view, the NO oxidation capacity of the sample $CeO_2(Ce^{4+})$ is the lowest one and its NO_2 profile is shifted towards higher temperatures with regard to the rest of the samples tested (Fig. 4b). This finding is in agreement with the trend reported in a previous publication [14], where at high calcination temperatures, and as a consequence of ceria sintering with decrease in surface area, the NO_x chemisorption and NO_2 production capacity became retarded and lowered in magnitude compared to the non-sintered ceria. The current results also support our recent conclusions of a work where it was observed that one of the key features governing the activity for NO_2 production was the ceria/zirconia ratio of the mixed oxides [28], cerium rich mixed oxides being more active than those with high Zr proportion. For the specific case of a pure ceria and a $Ce_{0.76}Zr_{0.24}O_2$ mixed oxide, both prepared from a Ce^{3+} precursor, their catalytic activities were very similar [28] as found in the present publication.

The catalytic activity for NO oxidation of the samples CeO_2 (Ce^{3+}), $Ce_{0.80}Zr_{0.20}O_2$ (Ce^{3+}) and $Ce_{0.80}Zr_{0.20}O_2$ (Ce^{4+}) is quite similar (Fig. 4b), but there are few differences that merit attention. By a careful comparison of the behaviour of ceria–zirconia mixed oxides, a slight difference is observed. Even though $Ce_{0.80}Zr_{0.20}O_2$ (Ce^{3+}) presents higher BET surface area than $Ce_{0.80}Zr_{0.20}O_2$ (Ce^{4+}), the NO_2 production capacity of the former sample is slightly lower than that of the latter. This proves that the surface area might not be the only cause to explain the activity of ceria–zirconia for NO oxidation, even though solids with identical nominal composition are compared. This slightly different behaviour concerning NO_2 production by the mixed oxides could be tentatively ascribed to the very different surface atomic distribution measured for both samples, which is related with the structure of the mixed oxides. The previously described characterization techniques showed that $Ce_{0.80}Zr_{0.20}O_2$ (Ce^{3+}) presents a ceria-like surface structure with an important Ce-enrichment on the surface. Meanwhile, $Ce_{0.80}Zr_{0.20}O_2$ (Ce^{4+}) is characterised by a single structure t″ with a Zr-enriched outer layer, thus facilitating one or more of the following steps involved in the NO to NO_2 oxidation mechanism: $(NO + O_2)$ adsorption over the catalyst surface, oxidation of the ad-NO_x species formed and NO_2 release under $(NO + O_2)$. The different routes leading to ad-NO_x species formation/oxidation/desorption over ceria and ceria–zirconia samples are very complex and were explored in the previous work [28], being very dependent on the ceria–zirconia ratio of the samples considered. To sum up, the experimental results obtained in this study suggest that the higher NO oxidation capacity of the sample $Ce_{0.80}Zr_{0.20}O_2$ (Ce^{4+}) in comparison with $Ce_{0.80}Zr_{0.20}O_2$ (Ce^{3+}) could be attributed to their very different Ce/Zr surface ratios, and probably, to the improved redox properties of the former sample, as deduced from H_2-TPR experiments (Fig. 3).

4. Conclusions

In this study, the influence of the cerium precursor on the physico-chemical features and NO to NO_2 oxidation capacity of ceria and ceria–zirconia catalysts has been evaluated, and the following conclusions can be summarised:

- The cerium precursor, either $Ce(NO_3)_3{\cdot}6H_2O$ or $(NH_4)_2Ce(NO_3)_6$, affects significantly the physico-chemical features of ceria and ceria–zirconia mixed oxides prepared by coprecipitation, and this, in turn, affects the NO oxidation capacity of the oxides obtained.
- The precursor $Ce(NO_3)_3{\cdot}6H_2O$ (with Ce^{3+}) leads to a Ce–Zr mixed oxides with ceria-like structure and heterogeneous distribution of cerium and zirconium, with Ce-enrichment on the particle surface.
- In contrast, a Ce–Zr solid solution with t″ structure was achieved by using $(NH_4)_2Ce(NO_3)_6$ (with Ce^{4+}), which is similar to that of a commercial catalyst characterised as reference material. The Ce–Zr solid solution prepared from the precursor $(NH_4)_2Ce(NO_3)_6$ shows the highest NO oxidation capacity among the samples prepared in this study.
- For pure ceria samples, the effect of the cerium precursor is opposite to that described for the Ce–Zr mixed oxides. Pure ceria obtained from $(NH_4)_2Ce(NO_3)_6$ sinters during calcination more than ceria obtained from $Ce(NO_3)_3{\cdot}6H_2O$. As a consequence, ceria prepared from $(NH_4)_2Ce(NO_3)_6$ presents lower surface area, depleted redox properties and lower NO oxidation capacity than ceria prepared from $Ce(NO_3)_3{\cdot}6H_2O$.

Acknowledgments

The authors wish to acknowledge the financial support provided by the Spanish Ministry of Science and Innovation (project CTQ-2009-07475) and the Generalitat Valenciana within the framework of Prometeo Programme (Prometeo/2009/047 project). N.G.H. gratefully acknowledges Vicerrectorado de Investigación, Desarrollo e Innovación (University of Alicante) for her Ph.D. grant.

References

[1] A. Trovarelli (Ed.), Catalysis by Ceria and Related Materials, Catalytic Science Series, vol. 2, Imperial College Press, 2002, pp. 51–83.
[2] Y. Madier, C. Descorme, A.M. Le Govic, D. Duprez, J. Phys. Chem. 103 (1999) 10999–11006.
[3] F. Zamar, A. Trovarelli, C. de Leitenburg, G. Dolcetti, J. Chem. Soc. Chem. Commun. (1995) 965–966.
[4] L.V. Mattos, E.R. Oliveira, D.E. Resasco, F.B. Passos, F.B. Noronha, Fuel Process Technol. 83 (2003) 147–161.
[5] L.V. Mattos, E.R. Oliveira, P.D. Resende, F.B. Noronha, F.B. Passos, Catal. Today 77 (2002) 245–256.
[6] A. Setiabudi, J. Chen, G. Mul, M. Makkee, J.A. Moulijn, Appl. Catal. B 51 (2004) 9–19.
[7] A. Setiabudi, M. Makkee, J.A. Moulijn, Appl. Catal. B 50 (2004) 185–194.
[8] I. Atribak, I. Such-Basáñez, A. Bueno-López, A. García-García, J. Catal. 250 (2007) 75–84.
[9] W.S. Epling, L.E. Campbell, A. Yezerets, N.W. Currier, J.E. Parks, Catal. Rev. Sci. Eng. 46 (2004) 163–245.
[10] C. Thomas, O. Gorce, F. Villain, G. Djega-Mariadassou, J. Mol. Catal. A: Chem. 249 (2006) 71–79.
[11] http://www.platinum.matthey.com/.
[12] J. Kaspar, P. Fornasiero, G. Balducci, R. di Monte, N. Hickey, V. Sergo, Inorg. Chim. Acta 349 (2003) 217–226.
[13] S. Letichevsky, C.A. Tellez, R.R. de Avillez, M.I.P. da Silva, M.A. Fraga, L.G. Appel, Appl. Catal. B 58 (2005) 203–210.
[14] I. Atribak, A. Bueno-López, A. García-García, J. Catal. 259 (2008) 123–132.
[15] A. Laachir, V. Perrichon, A. Badri, J. Lamotte, E. Catherine, J.C. Lavalley, J. El Fallal, L. Hilaire, F. le Normand, E. Quéméré, G.N. Sauvion, O. Touret, J. Chem. Soc., Faraday Trans. 87 (1991) 1601–1609.
[16] C.E. Hori, H. Permana, K.Y. Simon Ng, A. Brenner, K. Mre, K.M. Rahmoeller, D. Belton, Appl. Catal. B 16 (1998) 105–117.
[17] S. Rossignol, F. Gérard, D. Duprez, J. Mater. Chem. 9 (1999) 1615–1620.
[18] A. Martínez-Arias, M. Fernández-García, V. Ballesteros, L.N. Salamanca, J.C. Conesa, C. Otero, J. Soria, Langmuir 15 (1999) 4796–4802.
[19] M. Yashima, K. Korimoto, N. Ishizawa, M. Yoshimura, J. Am. Ceram. Soc. 76 (1993) 1745–1750.
[20] P. Fornasiero, J. Kaspar, M. Graziani, Appl. Catal. B 22 (1999) L11–L14.
[21] S. Bernal, J.J. Calvino, G.A. Cifredo, J.M. Gatica, J.A. Perez Omil, J.M. Pintado, J. Chem. Soc., Faraday Trans. 89 (1993) 3499–3505.
[22] P. Vidmar, P. Fornasiero, J. Kaspar, G. Gubitosa, M. Graziani, J. Catal. 171 (1997) 160–168.
[23] A.E. Nelson, K.H. Schulz, Appl. Surf. Sci. 210 (2003) 206–221.
[24] Y. Guo, G. Lu, Z. Zhang, S. Zang, Y. Qi, Y. Liu, Catal. Today 126 (2007) 296–302.
[25] X. Wu, L. Qing, W. Xiaodi, W. Duan, J. Rare Earth 25 (2007) 416–421.
[26] Y. Nagai, T. Yamamoto, T. Tanaka, S. Yoshida, T. Nonaka, T. Okamoto, A. Suda, M. Sugiura, Catal. Today 74 (2002) 225–234.
[27] N.N. Greenwood, A. Earnshaw, Chemistry of the Elements, 2nd ed., Elsevier, Butterworth–Heinemann, Oxford, MA, 2003.
[28] I. Atribak, B. Azambre, A. Bueno-López, A. García-García, Appl. Catal. B 92 (2009) 126–137.